Am J Transl Res 2021;13(6):5835-5850
www.ajtr.org /ISSN:1943-8141/AJTR0121852

Original Article

Long non-coding RNA H19 and the underlying epigenetic function in response to DNA damage of lung cancer cells

Dongjie Wang[1], Yajiao Sun[2], Lin Lin[2], Yulan Sang[1], Fan Yang[3], Jiawen Zhang[1], Li Jia[1], Ziping Xu[1], Wei Zhang[1]

[1]Department of Respiratory Medicine, The First Affiliated Hospital of Harbin Medical University, Harbin 150001, P. R. China; [2]Department of Respiratory Medicine, The Second Affiliated Hospital of Harbin Medical University, Harbin 150001, P. R. China; [3]Department of Neurology, The First Affiliated Hospital of Harbin Medical University, Harbin 150001, P. R. China

Received September 6, 2020; Accepted February 7, 2021; Epub June 15, 2021; Published June 30, 2021

Abstract: The purpose of the current study is to clarify the epigenetic function of long non-coding RNA (lncRNA) H19 in lung cancer as well as the relevant regulatory mechanism. We first determined H19 upregulation in A549 cells. DNA damage model was established in A549 cells by exposure to X-ray and then ionizing radiation (IR). The degree of DNA damage in the IR cell model was assessed by Comet assay. Gain- and loss-of-function assays were employed to clarify the roles of H19 and miR-675 in DNA damage of A549 cells. The results demonstrated that H19 knockdown inhibited the response of lung cancer cells to IR-induced DNA damage but promoted the damage repair. H19 could interact with miR-675, whereby aggravating IR-induced DNA damage. Furthermore, p62 was identified to be a downstream gene positively regulated by miR-675 while APEX1 was a target gene negatively regulated by miR-625-5p. Meanwhile, silencing of H19 could inhibit APEX1 expression by upregulating miR-625-5p, thereby accelerating DNA damage repair in A549 cells. In conclusion, H19 could function as a modulator of DNA damage response in lung cancer cells.

Keywords: Lung cancer, DNA damage response, epigenetic regulation, long non-coding RNA H19, microRNA-675, microRNA-625-5p, A549 cells

Introduction

Lung cancer is a common malignancy with high incidence globally [1]. It is reported that approximately 1.8 million cases are diagnosed as lung cancer annually while 1.6 million cases are related to cancer death [2]. Nevertheless, nearly 70% of lung cancer patients are unable to receive surgeries due to the metastatic property of lung cancer [3]. Therefore, in-depth understanding of molecular mechanism underlying cancer progression may be conductive to the development of therapeutic targets for lung cancer. Recently, DNA damage response has been investigated extensively since it functions as a maintainer of genomic integrity, which is crucial for cell viability [4]. Previous literature has documented that DNA damage is a factor influencing progression of lung cancer, which is closely associated with intrinsic DNA damage response machinery [5]. However, the relevant studies on the specific mechanism of DNA damage in lung cancer are limited. Molecular alterations including epigenetic aberrations mediate lung cancer development, which are implicated in DNA damage repair [6]. Moreover, epigenetic modifications are critical in regulating DNA methylation and non-coding RNAs (ncRNAs) interventions [7]. A deeper insight into the epigenetic regulation mechanism of lung cancer may contribute to identification of new targets for lung cancer therapy.

Long non-coding RNAs (lncRNAs) are RNA transcripts longer than 200 nucleotides, which are associated with the tumorigenesis of lung cancer [8]. H19 is considered as an oncogenic lncRNA which is commonly highly expressed in cancers [9]. Prior work has demonstrated the involvement of H19 in non-small cell lung can-

cer (NSCLC) [10]. It has been suggested in previous studies that c-Myc enhances the activity of H19 promoter [11], and that FOXF2 binds to the H19 promoter [12], resulting in upregulation of H19 in lung cancer. A prior study has proposed the function of H19 in erlotinib resistance of NSCLC [13]. However, the downstream how H19 affects response of lung cancer cells to DNA damage is rarely reported. Furthermore, H19 has been declared to regulate microRNA (miR)-675 in NSCLC [14]. miR-675 could accelerate NSCLC progression [15]. Moreover, miR-625-5p is also regulated by specific lncRNA LINC00958 in lung cancer, with the involvement in biological function of lung adenocarcinoma cells [16]. Based on the above-mentioned references, we aimed to explore the roles of H19 and miR-675/miR-625-5p in regulation of DNA damage response in lung cancer and corresponding downstream mechanism.

Materials and methods

Cell treatment

Human lung cell line BEAS-2B cells (Cell Bank of China Typical Culture Preservation Center; resource number: 3142C0001000000828) were cultured in high-glucose Dulbecco's modified eagle medium (DMEM with 214.5 g/Liter glucose) supplemented with 10% fetal bovine serum (FBS). Lung cancer A549 cells (Cell Resource Center of Institute of Basic Medical Sciences, Chinese Academy of Medical Sciences; resource number: 3142C0001000000062) were cultured in McCoy's 5A Media (Modified with Tricine) containing 10% FBS and incubated in 5% CO_2 at 37°C. DNA damage model was established when A549 cells were irradiated with 5 Gy of X-ray for 12 h, and then incubated for 8 h.

Cell transfection

The small interfering RNA (siRNA) of H19 was synthesized by Gene Tech (Shanghai, China) with sequences listed in Supplementary Table 1. Briefly, 1.2×10^7 cells were placed in a 15 cm dish for 24 h, and then transfected with the green fluorescent protein (GFP)-labeled miR-675 mimic, miR-675 inhibitor, and their corresponding negative controls (NCs) (RiboBio, Guangzhou, China) using Lipofectamine 2000 (Invitrogen; Thermo Fisher Scientific, Waltham, MA) for 24 h. RNA/protein was extracted from these cells to conduct further functional assays.

Dual-luciferase reporter gene assay

Binding sites between H19 and miR-675 were predicted by the bioinformatics website RNAInter (http://www.rna-society.org/rnainter/), while those between H19 and miR-625-5p by the Starbase website (http://starbase.sysu.edu.cn/). Targetscan website (http://www.targetscan.org/cgi-bin/targetscan/) was employed to obtain the binding sites of miR-625-5p and APEX1. The wild-type (WT) sequence containing the binding site of H19 was synthesized, based on which the mutation (MUT) sequence was constructed. Next, the WT or MUT of H19-binding miR-675 (or miR-625-5p) was cloned intopGL3 Basic vector (Promega, Madison, WI, USA). Then miR-675/miR-625-5p mimic was co-transfected with pGL3-WT-H19 or pGL3-MUT-H19 into HEK-293T cells. The promoter sequence on p62 was mutated, and WT or MUT p62-binding miR-675 was also cloned into pGL3 Basic vector. miR-675 was co-transfected with pGL3-WT-p62 or pGL3-MUT-p62. Similarly, APEX13' untranslated region (UTR) sequence was mutated, and WT or MUT APEX-binding miR-625-5p was cloned into pGL3 Basic vector. Luciferase activity was detected using a dual luciferase reporter assay system (Promega).

RNA binding protein immunoprecipitation (RIP)

A549 cells were fixed with 1% formaldehyde for 10 min and centrifuged at 1,500 × g and 4°C (5 min). Cell precipitates were lysed in NP-40 lysis buffer. Then, the supernatant was incubated with beads bound to AGO2 antibody (ab186733, 1:30; Abcam, Cambridge, UK) or NC immunoglobulin G (IgG) (ab205718, 1:50; Abcam). The beads were cultured with 10 mg/mL proteinase K (Sigma-Aldrich, St. Louis, MO, USA), and the total RNA was extracted from the obtained immunoprecipitants for reverse transcription-quantitative polymerase chain reaction (RT-qPCR).

RT-qPCR

Total RNA was obtained using RNAiso Plus technique (TaKaRaBio Technology, Dalian, China). For mRNA detection, 2 μg of total RNA was transcribed into cDNA using AMV reverse

transcriptase (Promega). miRNAs were detected using 2 μg of total RNA, miRNAs-specific stem-loop RT primers and MMLV reverse transcriptase (Promega). Reaction system was prepared by Fast SYBR Green PCR kit (Applied Biosystems, Grand Island, NY, USA), and RT-qPCR was conducted under an ABI 7900 real-time PCR detection system (Applied Biosystems). Glyceraldehyde-3-phosphate dehydrogenase (GAPDH) served as the internal reference for H19 and p62, while miR-675 and miR-625-5p were normalized to U6. Relative gene expression was analyzed by $2^{-\Delta\Delta}$Ct method. All primers are shown in Supplementary Table 2.

Western blot analysis

Cell lysates were prepared using RIPA buffer containing protease inhibitors (Sigma-Aldrich). Protein concentration in cell lysate was detected using a bicinchoninic acid (BCA) kit (Beyotime, Shanghai, China). An equal amount of protein samples was separated by 10% sodium dodecyl sulfate-polyacrylamide gel electrophoresis (SDS-PAGE) and transferred to polyvinylidene fluoride membrane (EMD-Millipore, New Jersey, USA). Being blocked by TBST buffer containing 5% skimmed milk powder for 2 h at ambient temperature, membranes were probed with primary antibodies (Abcam) including p62 (ab155686, 1:500), Caspase-3 (ab13847, 1:500), c-Caspase-3 (ab49822, 1:500), Chk1 (ab40866, 1:10000), phosphorylated-Chk1 (ab79758, 1:1000), APEX1 (ab183039, 1:200), and GAPDH (ab181602, 1:10000) overnight at 4°C. Secondary antibody horseradish peroxide (HRP)-labeled IgG (ab205718, 1:2000) was then added to the membrane for immune-staining at ambient temperature (1 h). Proteins were visualized by enhanced chemiluminescence detection system with Immobilon-Western chemiluminescent HRP substrate (EMD-Millipore).

Comet assay

DNA damage induced by ionizing radiation (IR) was evaluated by conducting Comet assay (also known as single cell gel electrophoresis) with reference to the instructions (Cell Biolabs Inc., San Diego, CA). Cells were trypsinized. Then, the OxiSelect comet slide was covered with a mixture of comet agarose and cells. After being lysed, the slides were electrophoresed at 1 V/cm and 4°C for 30 min, stained with Vista green DNA staining solution, and observed by fluorescence microscopy. The percentage of DNA migration in the tail (% of tail DNA), tail moment and tail length were analyzed by comet analysis software V4.3 (Perceptive Instruments, Suffolk, UK).

Flow cytometry

Cells transfected for 24 h were seeded in 6-well culture plates (5×10^5 cells/well). Then cells were trypsinized, resuspended with pre-cooled 70% ethanol, and fixed at -20°C. The next day, cells were centrifuged and resuspended in 100 μL binding buffer. Double staining of Annexin V-fluorescein isothiocyanate (FITC; 0.1 μg) and propidium iodide (PI, 10 μL, 50 μg/mL) was performed as per the manufacturer's protocols (BD Biosciences, CA, USA). Apoptosis was conducted using FACSCalibur flow cytometer (BD Biosciences) and CellQuest software within 1 h.

Immunofluorescence

Cells were seeded in immunofluorescent cell culture dishes. When cell confluency reached approximately 80%, cells were fixed with formaldehyde, treated with Triton X-100 and blocked with PBS containing 5% bovine serum albumin (BSA) for 1 h. Cells were then immune-stained with anti-histone H2AX phosphorylated (γ-H2AX) antibody (ab195189, 1:200; Abcam) overnight at 4°C. Next, cells were added with Alexa Fluor 647-labeled secondary antibody IgG (ab150075, 1:200; Abcam) for 1 h at ambient temperature. Immunofluorescence was performed using a laser scanning confocal microscope (Olympus Optical, Tokyo, Japan). At least 50 cells were evaluated for each sample and the number of positive cells was counted.

Co-immunoprecipitation (IP)

Cells were lysed with 1 mL whole-cell extraction buffer A (50 mM; pH = 7.6 Tris-HCl, 150 mM NaCl; 1% NP40; 0.1 mM EDTA; 1.0 mM DTT; 0.2 mM PMSF; 0.1 mM Pepstatine; 0.1 mM Leupeptine, and 0.1 mM Aproine). Protein concentration was determined by BCA method. Part of lysate served as Input, while the same amount of total protein was removed from the remaining lysate. Each sample was added with 2 μg antibodies against hMSH6 (ab208940, 1:40), CREB (ab32525, 1:80), and IgG

(ab205718, 1:50) and quantitative Protein A&G, which was incubated at 4°C in vortex. The next day, the precipitate was collected by centrifugation, washed five times with detergent (50 mM pH 7.6 Tris Cl, 150 mM NaCl; 0.1% NP-40; and 1 mM EDTA) with 10 min each time, and then resuspended in 60 μL 2 × SDS-PAGE sample loading buffer, followed by Western blot analysis.

Chromatin IP (ChIP)

Cells were cross-linked with 1% (v/v) formaldehyde (Sigma-Aldrich) (10 min) at ambient temperature, treated with 125 mm glycine (5 min), resuspended in lysis buffer, and then placed in an ultrasonic shaker for 8-10 min to produce DNA fragments with an average size of about 500 bp. Chromatin extract was diluted 5 times, and incubated with equal amounts of Protein A&G and antibody overnight at 4°C. The antibodies to CREB (ab32525, 1:80), P300 (a14984, 1:50), and IgG (ab205718, 1:50) as NC were used in this experiment.

Statistical analysis

All data were analyzed using SPSS 21.0 statistical software (IBM Corp., Armonk, NY, USA), and the measurement data were summarized by mean ± standard deviation, with $P < 0.05$ as a level of statistically significance. Independent sample *t*-test was used for comparison between two groups, whereas one-way analysis of variance (ANOVA) was used for comparisons among multiple groups with Tukey's post-test used.

Results

H19 knockdown suppress DNA damage induced by IR

As shown in **Figure 1A**, RT-qPCR demonstrated elevated H19 expression in A549 cells relative to BEAS-2B cells. To clarify the role of H19 on DNA damage, we induced cellular DNA damage models using IR-treated A549 cell line. The degree of DNA damage was assessed by Comet assay (**Figure 1B**). Compared with the untreated cells, tail DNA, tail length, and tail moment were strikingly enhanced in the IR-induced A549 cells, indicating the successful establishment of IR cell model.

Then, interference efficiency of siRNAs against H19 in IR lung cancer cells was validated by RT-qPCR (**Figure 1C**). Results displayed that the si-H19-3 with the lowest expression of H19 was chosen for further experiment. Next, IR-induced cell death was detected by flow cytometry in cells after silencing or overexpressing H19, results of which revealed distinctly reduced apoptosis rate in the si-H19-treated cells (**Figure 1D**). Moreover, levels of Caspase-3, c-Caspase-3, and DNA damage response proteins Chk1 and phosphorylated-Chk1 were detected by Western blot analysis (**Figure 1E**). Treatment of si-H19 led to reduced levels of c-Caspase-3 and phosphorylated-Chk1. As immunofluorescence results revealed, level of DNA damage marker γ-H2AX was decreased by si-H19 (**Figure 1F**). As reflected by Co-IP results (**Figure 1G**), downregulation of H19 promoted the interaction between hMSH6 and H3K36me3, as well as that between hMSH6 and SKP2 in the damage repair protein complex.

H19 interacts with miR-675

Interacted regulators of H19 were predicted by the bioinformatics website RNAInter (**Figure 2A**). It was shown that the interaction score between miR-675 and H19 was the highest (Score = 1). The binding sites between H19 and miR-675 were obtained by RNAInter (**Figure 2B**). Moreover, the binding relationship between H19 and miR-675 was verified using RIP assay, the results of which showed that both H19 and miR-675 recruited by Ago2 were markedly increased (**Figure 2C**). Dual-luciferase reporter gene assay further confirmed that luminescent signal was elevated when miR-675 mimic was co-transfected with H19-WT (**Figure 2D**). In addition, RT-qPCR results displayed that miR-675 expression was suppressed by si-H19, while overexpressed H19 induced miR-675 expression (**Figure 2E**).

Downregulated miR-675 facilitates DNA damage repair of lung cancer cells

RT-qPCR revealed that compared with BEAS-2B cells, miR-675 expression was upregulated in A549 cells (**Figure 3A**). Subsequently, miR-675 was downregulated in IR-induced lung cancer cells using miR-675 inhibitor (**Figure 3B**). The results of flow cytometry showed that the apoptosis rate reduced after miR-675 was downregulated by miR-675 inhibitor (**Figure 3C**). In addition, Western blot analysis results revealed

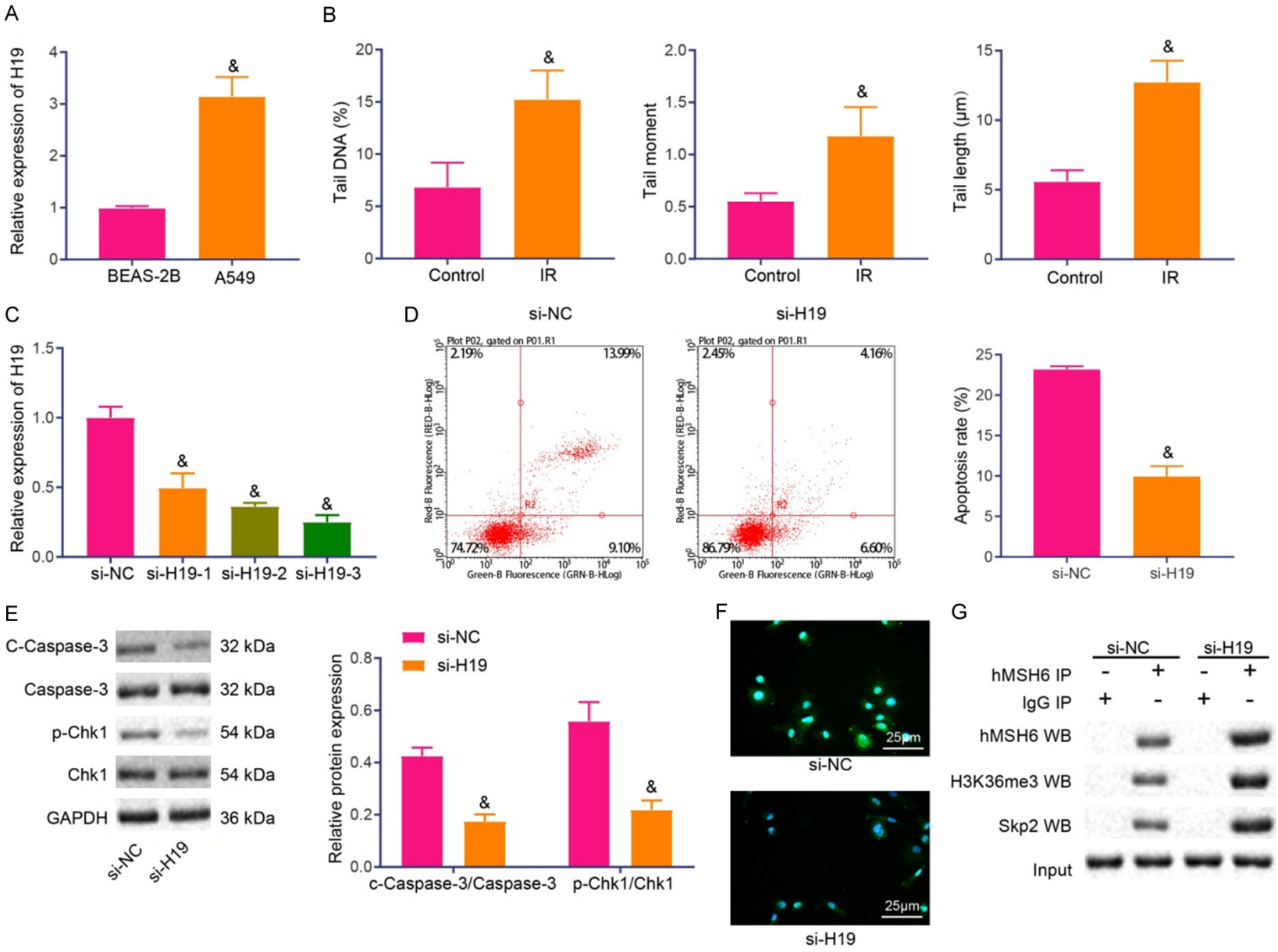
A
Relative expression of H19
BEAS-2B
A549
B
Tail DNA (%)
Control
IR
Tail moment
Tail length (μm)
C
Relative expression of H19
si-NC
si-H19-1
si-H19-2
si-H19-3
D
si-NC
si-H19
Plot P02, gated on P01.R1
2.19%
13.99%
74.72%
9.10%
2.45%
4.16%
86.79%
6.60%
Red-B Fluorescence (RED-B-HLog)
Green-B Fluorescence (GRN-B-HLog)
Apoptosis rate (%)
E
C-Caspase-3
Caspase-3
p-Chk1
Chk1
GAPDH
32 kDa
54 kDa
36 kDa
Relative protein expression
c-Caspase-3/Caspase-3
p-Chk1/Chk1
F
25μm
G
hMSH6 IP
IgG IP
hMSH6 WB
H3K36me3 WB
Skp2 WB
Input

Figure 1. H19 knockdown reduces DNA damage and promotes damage repair in lung cancer cells. A. Expression of H19 in BEAS-2B cells and A549 cells determined using RT-qPCR. B. Degree of DNA damage in IR cell model evaluated using Comet assay. C. Silencing efficiency of si-H19-1, si-H19-2, and si-H19-3 in IR-exposed lung cancer cells determined using RT-qPCR. D. Apoptosis rate of IR-exposed lung cancer cells after silencing H19 analyzed using flow cytometry. E. Levels of c-Caspase-3/Caspase-3 and phosphorylated-Chk1/Chk1 detected using Western blot analysis. F. Immunofluorescence results of the level of the DNA damage marker γ-H2AX in IR-exposed lung cancer cells after silencing of H19 (200 ×). G. Co-IP results of the interaction between hMSH6 and H3K36me3, hMSH6 and SKP2 in IR-exposed lung cancer cells silencing H19. &$P < 0.05$ compared with BEAS-2B group or control group or si-NC group. A, B, and E. Comparisons are made using independent sample *t* test. C. Comparison is performed using one-way ANOVA. Cellular experiment is repeated three times.

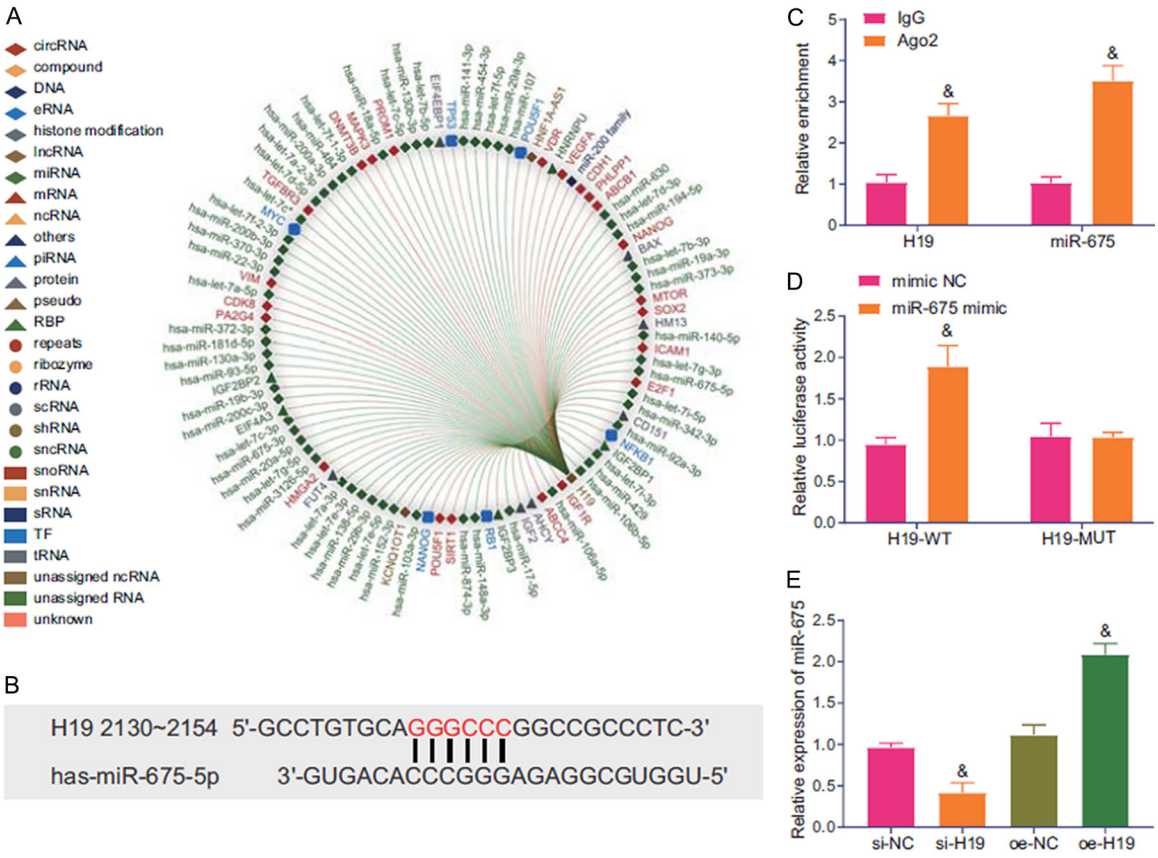

Figure 2. H19 specifically binds to miR-675. A. Interacted regulatory factors of H19 predicted by RNAInter website (http://www.rna-society.org/rnainter/). B. Binding sites between H19 and miR-675 predicted by RNAInter website. C. Binding relationship between H19 and miR-675 verified using RIP assay. D. Binding sites between H19 and miR-675 predicted by dual-luciferase reporter gene assay. E. Expression of miR-675 in A549 cells overexpressing or silencing H19 determined using RT-qPCR. &$P < 0.05$ compared with IgG group, mimic NC, si-NC or oe-NC. Comparisons are made using independent sample *t* test. Cellular experiment is repeated three times.

silenced miR-675 decreased the protein expression of c-Caspase-3 and phosphorylated-Chk1 (**Figure 3D**). Immunofluorescence results displayed reduced γ-H2AX level after miR-675 inhibition (**Figure 3E**). Co-IP results presented that miR-675 inhibitor promoted the interaction between hMSH6 and H3K36me3, as well as between hMSH6 and SKP2 (**Figure 3F**).

Silenced miR-675 suppresses p62 expression

Next, we screened the downstream regulators of miR-675. There were 4930 target genes of

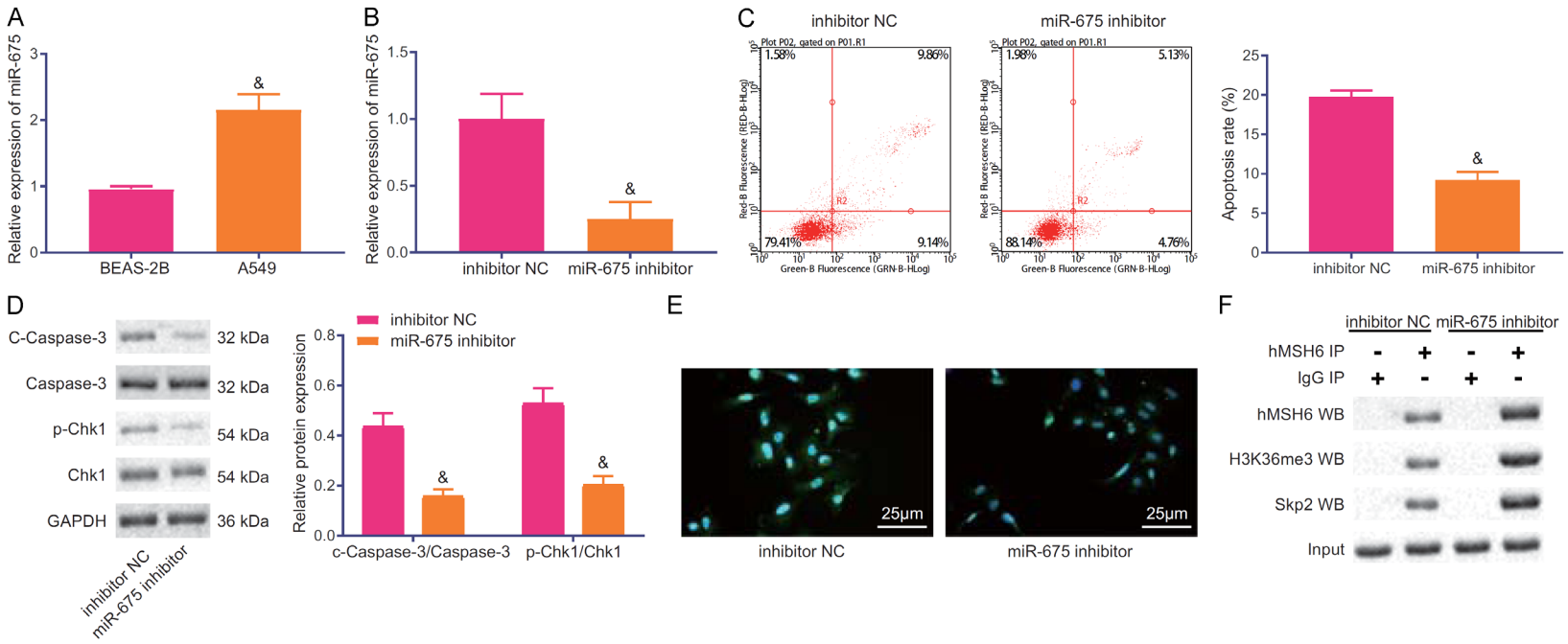

Figure 3. Downregulation of miR-675 promotes DNA damage repair. A. Expression of miR-675 in BEAS-2B and A549 cells determined using RT-qPCR. B. Expression of miR-675 in IR-exposed lung cancer cells determined using RT-qPCR. C. Apoptosis of IR-exposed lung cancer cells after silencing of miR-675 evaluated using flow cytometry. D. Protein expression of Caspase-3, c-Caspase-3, Chk1, and phosphorylated-Chk1 determined by Western blot analysis after silencing of miR-675. E. DNA damage marker expression detected using immunofluorescence (200 ×). F. Interaction between hMSH6 and H3K36me3, or hMSH6 and SKP2 assessed by Co-IP after silencing of miR-675. &$P < 0.05$ compared with BEAS-2B cells or inhibitor NC. Comparisons are made using independent sample *t* test. Cellular experiment is repeated three times.

miR-675 predicted by the bioinformatics website miWalk, and 851 lung cancer-related genes as the GeneCards database shown. A total of 214 genes were obtained from the intersection (**Figure 4A**). The protein-protein interaction (PPI) network among 214 genes was obtained using the Coexpedia website (**Figure 4B**), of which 48 genes were co-expressed (Score > 50). Moreover, the heat map of 48 candidate gene expression was shown in TCGA database of lung cancer through UALCAN (**Figure 4C**), among which SQSTM1 (p62) was expressed at a high level in lung cancer samples (**Figure 4D**). Consistently, RT-qPCR revealed that p62 expression was higher in A549 cells than that in BEAS-2B cells (**Figure 4E**). We further investigated the regulation of p62 expression by miR-675 in lung cancer cells. RT-qPCR and Western blot results revealed that p62 level was suppressed by miR-675 inhibitor (**Figure 4F**, **4G**).

H19 exerts regulatory effects on DNA damage of lung cancer cells through miR-675/p62

Furthermore, we explored the effects of regulatory relationships among H19, miR-675, and p62 on response of lung cancer cells to DNA damage. RT-qPCR results showed that miR-675 and p62 were downregulated after H19 was knocked down by si-H19. However, p62 was increased when miR-675 was overexpressed in the H19-deficient cells (**Figure 5A**). Similarly, flow cytometric results showed that the apoptosis rate was restrained by si-H19, while the inhibitory effect of si-H19 on apoptosis was attenuated by miR-675 mimic (**Figure 5B**). Western blot results revealed that silenced H19 resulted in decreased levels of c-Caspase-3 and phosphorylated-Chk1, while overexpression of miR-675 reversed the effect of silenced H19 on the protein levels of c-Caspase-3 and phosphorylated-Chk1 (**Figure 5C**). Immunofluorescence results unraveled that silencing of H19 reduced the expression of γ-H2AX, yet gain-of-function of miR-675 abrogated the inhibitory effect of silencing H19 on γ-H2AX level (**Figure 5D**). Co-IP assay further showed that miR-675 mimic counteracted the promotion effect of si-H19 on the interactions between hMSH6 and H3K36me3 and between hMSH6 and SKP2 (**Figure 5E**).

H19 upregulates APEX1 by suppressing miR-625-5p expression

The binding sites between H19 and miR-625-5p were predicted by Starbase website (**Figure 6A**). In addition, we also found that miR-625-5p could bind to APEX1 through TargetScan database (**Figure 6B**). Therefore, we explored whether H19 could regulate the downstream miR-625-5p/APEX1 pathway to regulate the response of lung cancer cells to DNA damage. RT-qPCR showed that miR-625-5p was significantly underexpressed in A549 cells, while APEX1 was prominently upregulated (**Figure 6C**). Dual luciferase assay verified the binding of miR-625-5p to H19, and that of miR-625-5p to APEX1 (**Figure 6D**). It was found that the luminescent signal was weakened in the co-transfection of miR-625-5p mimic with H19-WT or with APEX1-WT. It was further shown by RIP assay that H19, miR-625-5p, and APEX1 recruited by Ago2 were increased. After silencing of H19, there were less H19 and more APEX1 recruited by Ago2 compared with IgG (**Figure 6E**). Western blot results displayed that silenced H19 upregulated miR-625-5p, while downregulated APEX1. However, downregulation of miR-625-5p significantly reversed the reduced APEX1 expressed induced by silenced H19 (**Figure 6F**).

H19 participates in the response to DNA damage of lung cancer cells via APEX1

Last, we explored the mechanism of H19/APEX1 in the response of lung cancer cells to DNA damage. RT-qPCR showed that miR-625-5p expression was enhanced but H19 and APEX1 were downregulated after si-H19 treatment, whereas expression of APEX1 distinctly increased upon additional treatment with oe-APEX1 (**Figure 7A**). Flow cytometry revealed that APEX1 overexpression attenuated the inhibitory effect of si-H19 on cellular apoptosis (**Figure 7B**). Western blotting further validated that silenced H19 reduced protein levels of c-Caspase-3 and phosphorylated-Chk1, which were rescued upon overexpression of APEX1 (**Figure 7C**). Immunofluorescence showed that loss of H19 reduced the expression of γ-H2AX, while overexpressing APEX1 diminished the inhibitory effect of silenced H19 on γ-H2AX expression (**Figure 7D**). Co-IP results indicated that oe-APEX1 counteracted the promotion effect of si-H19 on the interactions between hMSH6 and H3K36me3 and between hMSH6 and SKP2 (**Figure 7E**).

Discussion

LncRNAs are demonstrated to be crucial for DNA damage response, which mediate various

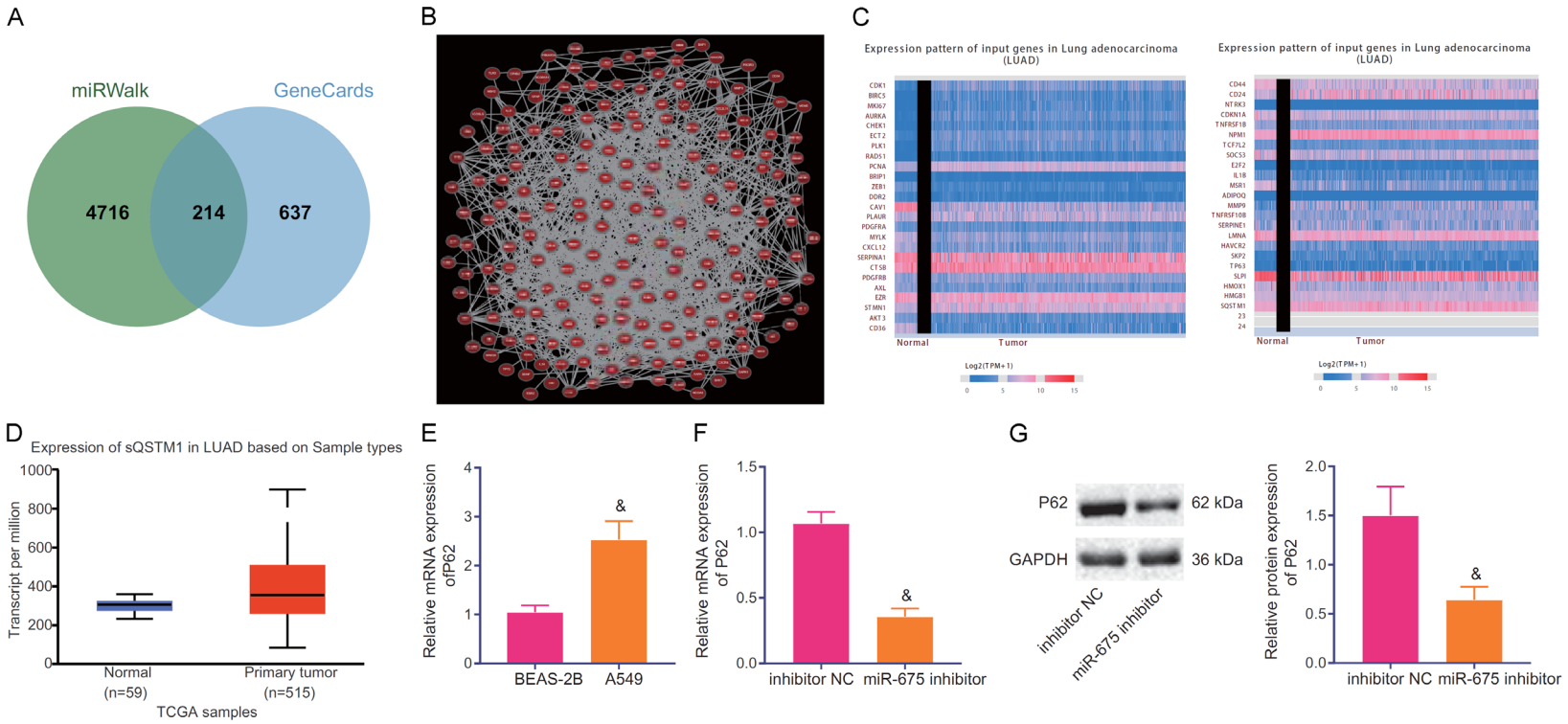

Figure 4. Overexpressed miR-675 promotes p62 expression. A. Intersection of interacted genes predicted by miWalk (http://mirwalk.umm.uni-heidelberg.de/) with lung cancer-related genes predicted by GeneCards (https://www.genecards.org/). B. PPI network of 214 genes obtained by Coexpedia (http://www.coexpedia.org/). C. Expression of 48 candidate genes in lung cancer shown in TCGA database obtained by UALCAN (http://ualcan.path.uab.edu/). D. Expression of p62 in lung cancer obtained from TCGA database. E. p62 expression in BEAS-2B and A549 cells determined using RT-qPCR. F. p62 mRNA expression in A549 cells after silencing of miR-675 determined using RT-qPCR. G. p62 protein expression in A549 cells after silencing of miR-675 measured using Western blot analysis. &$P < 0.05$ compared with BEAS-2B cells or inhibitor NC. Comparisons are made using independent sample *t* test. Cellular experiment is repeated three times.

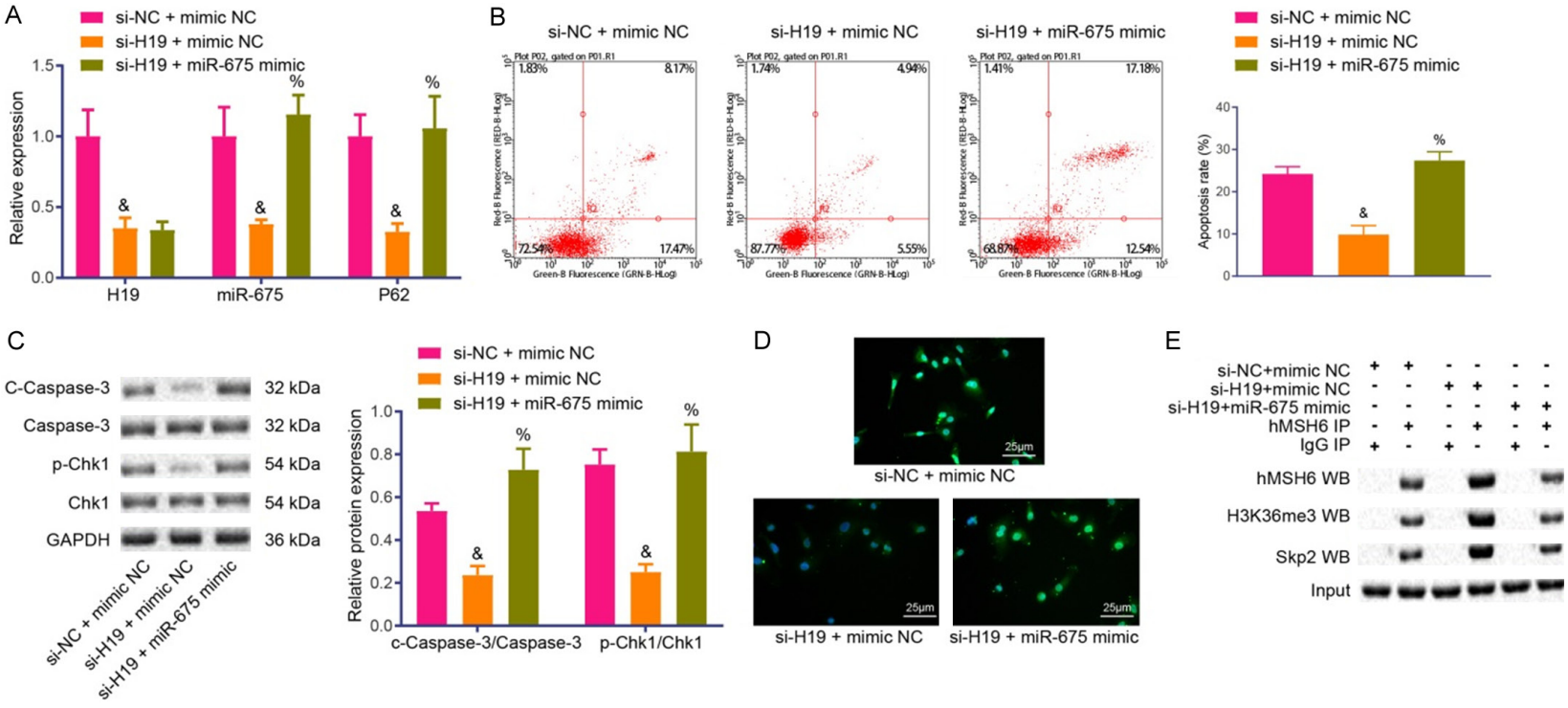

Figure 5. H19 regulates response of lung cancer cells to DNA damage through miR-675/p62. A. Expression of H19, miR-675, and p62 in IR-exposed lung cancer cells after co-treatment of si-H19 and miR-675 mimic determined using RT-qPCR. B. Apoptosis rate of IR-exposed lung cancer cells after co-treatment of si-H19 and miR-675 mimic evaluated by flow cytometry. C. Protein levels of c-Caspase-3, Caspase-3, Chk1, and phosphorylated-Chk1 assessed by Western blot analysis after co-treatment of si-H19 and miR-675 mimic. D. Expression of γ-H2AX in IR-exposed lung cancer cells treated with si-H19 and miR-675 mimic determined using immunofluorescence (200 ×). E. Interactions between hMSH6 and H3K36me3 and between hMSH6 and SKP2 in IR-exposed lung cancer cells treated with si-H19 and miR-675 mimic determined using Co-IP. &$P < 0.05$ compared with si-NC + mimic NC. %$P < 0.05$ compared with si-H19 + mimic NC. Comparison is performed using one-way ANOVA. Cellular experiment is repeated three times.

A

miRNA	GeneID	GeneName	GeneType	TargetSite	Alignment	Class	AgoExpNum	CleaveExpNum	Pan-Cancer
hsa-miR-625-5p	ENSG00000130600	H19	processed_transcript	chr11:2016732-2016752[-]	Target: 5' uccacgacucugUUUCCCCCg 3' miRNA : 3' ccugauaucuugAAAGGGGGa 5'	7mer-m8	12	0	7

B

	Predicted consequential pairing of target region (top) and miRNA (bottom)	Site type	Context++ score	Context++ score percentile	Weighted context++ score	Conserved branch length	P_{CT}
Position 766-772 of APEX1 3' UTR hsa-miR-625-5p	5' ... GAUAAGUCCCUAACCUCCCCCAA ... 3' CCUGAUAUCUUGAAAGGGGGA	7mer-A1	-0.30	91	0.00	0	N/A

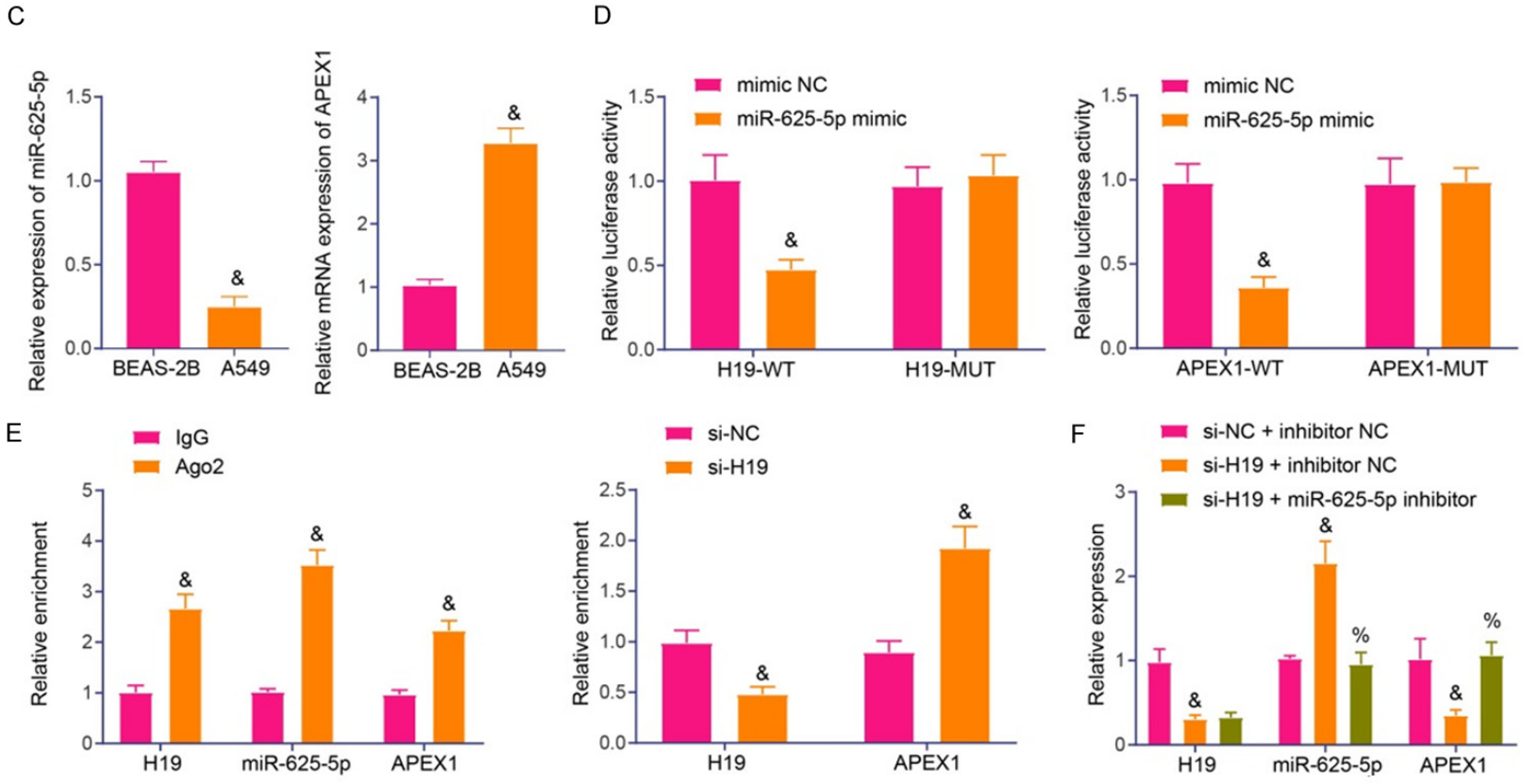

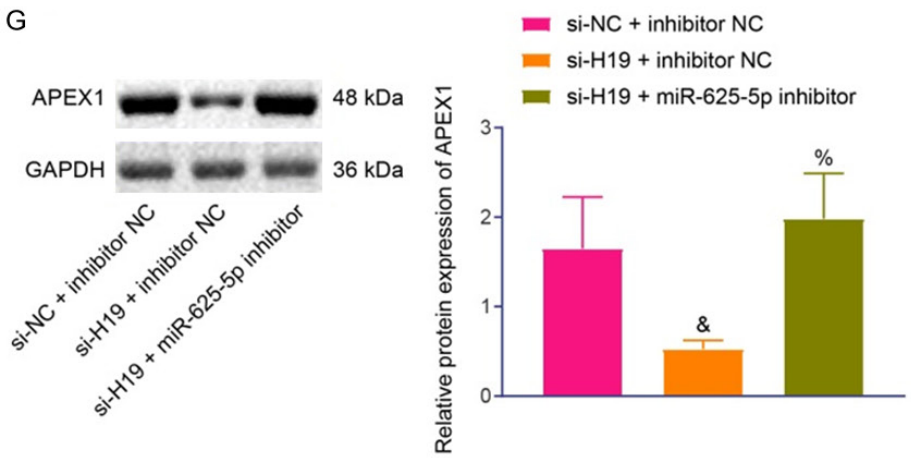

Figure 6. H19 promotes APEX1 expression by downregulating miR-625-5p. A. Binding sites between H19 and miR-625-5p predicted by starBase website. B. Binding sites between miR-625-5p and APEX1 predicted by TargetScan database. C. Expression of miR-625-5p, APEX1, and H19 in BEAS-2B and A549 cells determined using RT-qPCR. D. Binding relationship among H19, miR-625-5p, and APEX1 verified using dual-luciferase reporter gene assay. E. Interactions among H19, miR-625-5p, and APEX1 analyzed using RIP. F. Expression of miR-625-5p, APEX1, and H19 in lung cancer cells treated with si-H19 and miR-625-5p inhibitor determined using RT-qPCR. G. APEX1 protein expression in lung cancer cells treated with si-H19 and miR-625-5p inhibitor measured using Western blot analysis. &$P < 0.05$ compared with BEAS-2B cells, mimic NC or si-NC + inhibitor NC. %$P < 0.05$ compared with si-H19 + inhibitor NC. C-E. Comparisons are conducted using independent sample t test. F and G. Comparisons are conducted by one-way ANOVA. Cellular experiment is repeated three times.

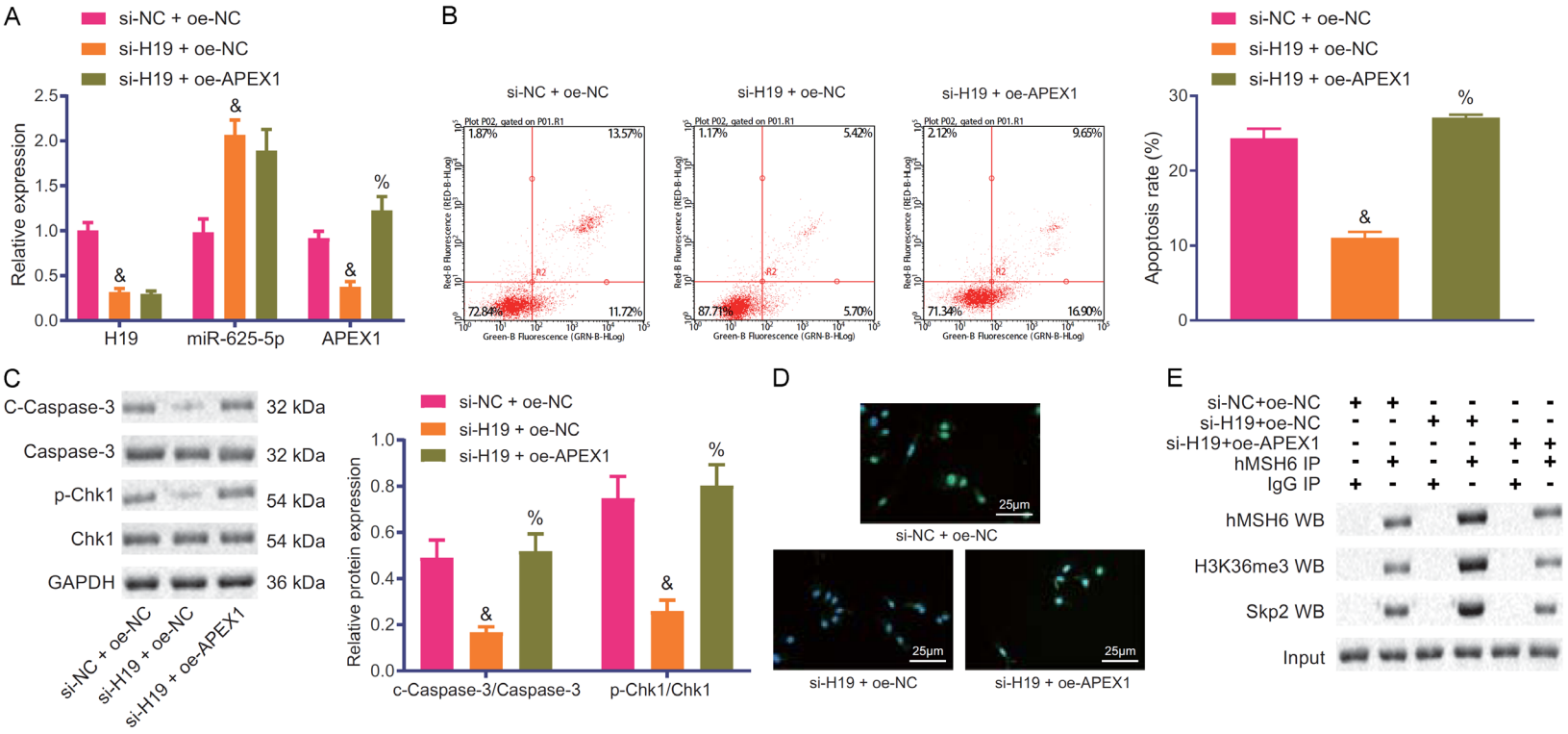

Figure 7. H19 mediates DNA damage repair through APEX1. A. Expression of H19, miR-675, and p62 in IR-exposed lung cancer cells after silencing H19 and overexpressing APEX1 determined using RT-qPCR. B. Apoptosis rate of IR-exposed lung cancer cells after silencing H19 and overexpressing APEX1 evaluated by flow cytometry. C. Protein levels of c-Caspase-3, Caspase-3, Chk1, and phosphorylated-Chk1 assessed by Western blot analysis after co-treatment of si-H19 and oe-APEX1. D. Expression of γ-H2AX in IR-exposed lung cancer cells treated with si-H19 and oe-APEX1 determined using immunofluorescence (200 ×). E. Interactions between hMSH6 and H3K36me3 and between hMSH6 and SKP2 in IR-exposed lung cancer cells treated with si-H19 and oe-APEX1 determined using Co-IP. &$P < 0.05$ compared with si-NC + oe-NC. %$P < 0.05$ compared with si-H19 + oe-NC. Comparison is performed using one-way ANOVA. Cellular experiment is repeated three times.

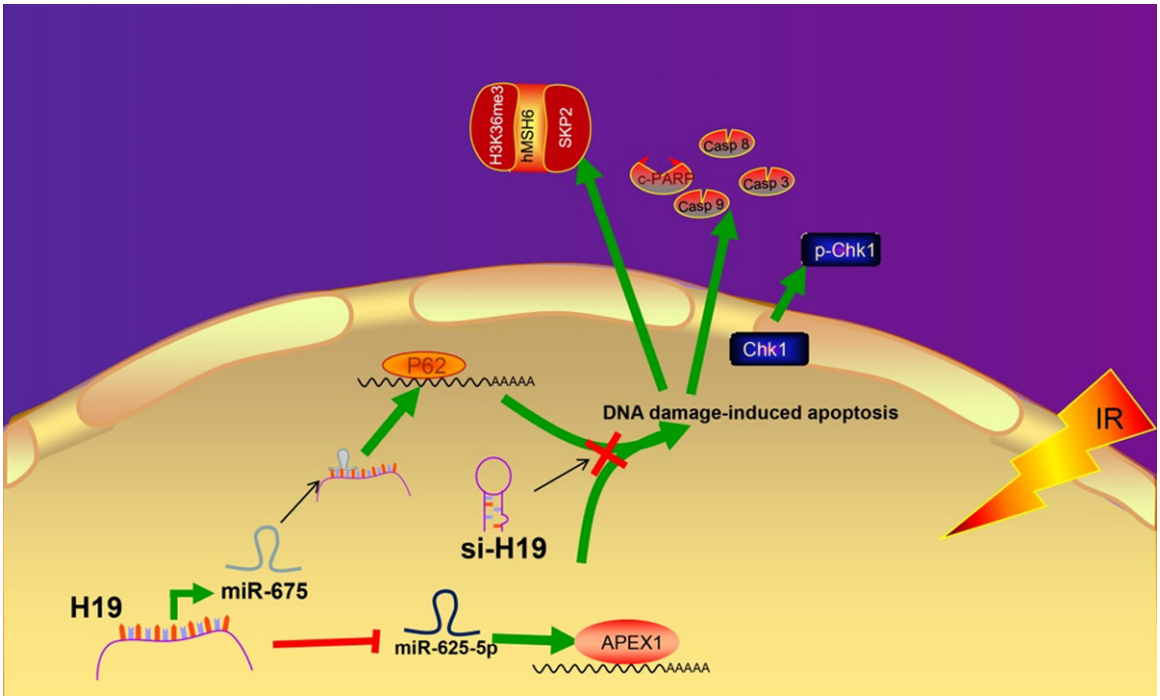

Figure 8. H19 promotes IR-induced DNA damage of lung cancer cells through promotion of APEX1 expression by downregulating miR-625-5p or promotion of p62 expression by upregulating miR-675.

cellular processes [17]. But the specific effects of lncRNAs on DNA damage response of lung cancer cells are still under exploration. It is reported that almost 90% of lung cancers are NSCLC [18]. Therefore, we mainly used lung cancer cell line A549 in the current study to establish the IR cell model. Moreover, we identified H19 as a promoter of DNA damage in lung cancer (**Figure 8**).

In our research, H19 enrichment occurred in A549 cells. Similarly, previous work also reports that H19 is highly expressed in epithelial ovarian cancer, due to epigenetic modification [19]. What's more, H19 is apparently upregulated in NSCLC, which exerts a promoting function on growth dynamics of lung cancer cells by targeting miR-17 [20, 21]. As manifested by the data collected from our study, knockdown of H19 downregulated protein levels of c-Caspase-3, phosphorylated-Chk1, and γ-H2AX. Based on existing report, Chk1 is a checkpoint for DNA damage, which is phosphorylated on Serine 345 (S345) in response to IR [22]. Moreover, phosphorylated-Chk1 is commonly induced by DNA damage response [23]. γ-H2AX is a member X of H2A histone family, the expression of which can be enhanced in IR dose-dependent fashion [24]. These studies support our statement that H19 promoted DNA damage induced by IR.

Mechanically, we found through bioinformatics analysis that H19 targeted miR-675, which further upregulated p62 level. It has been reported that certain lncRNAs can encode miRNAs and work together to achieve regulatory functions, while miR-675-5p is encoded by H19.

Moreover, the lncRNA-miRNAs regulatory pathway (H19-miR-675) regulates mRNA expression by directly interacting with miRNAs [25]. H19/miR-675 gene locus is also reported previously, which is considered as potential target for lung cancer treatment [26]. We further found that silenced miR-675 promoted DNA damage repair. Consistent with our study, researchers have declared that miR-675 contributes to the pathogenesis of lung cancer [27]. As **Figure 3F** shown, loss of miR-675 promoted the interaction among hMSH6, H3K36me3, and SKP2. It is revealed previously that miR-675 could upregulate polyubiquitin-binding protein p62 level, which binds to histone H3 and then reduces SETD2-binding capacity to substrate histone H3, therefore reducing expression of H3K36me3 [28]. Likewise, our data also showed that the H3K36me3-hMSH6-SKP2 triplex complex was decreased by miR-675 targeting p62. Accumulation of p62 (also known as SQSTM1) is reported to suppress DNA repair [29]. Our study also displayed that silenced miR-675 promoted p62 expression to enhance DNA damage repair.

Additionally, we also identified that H19 could bind to miR-625-5p in lung cancer. miR-625-5p could be regulated by lncRNA to affect the expression of CPSF7 in the process of lung cancer [16]. Furthermore, in A549 cells, miR-625-5p is poorly expressed, which is directly targeted by lncRNA MIR503HG [30]. Our bioinformatics analysis revealed that H19 increased APEX1 expression by suppressing miR-625-5p expression. Expression of APEX1 is demonstrated to be correlated with DNA damage repair, which is a diagnostic biomarker for hepatocellular cancer [31]. Being in line with our study, APEX1 is also proven to be highly expressed in NSCLC [32]. These works cooperatively support our finding that H19 boosts DNA damage response in association with miR-625-5p/APEX1 in A549 cells.

In conclusion, the evidence derived from our study showed that H19 promoted DNA damage in lung cancer. In contrast, depletion of H19 suppressed DNA damage and facilitated DNA damage repair. Thus, we surmised that silencing of H19 may be a potential therapeutic target for lung cancer treatment. However, *in vivo* assay is further required to attest to our assumption. Moreover, the correlation of H19 with clinical relevance has rarely been reported. More detailed functions of H19 in lung cancer treatment should be explored in the future.

Acknowledgements

We would like to give our sincere appreciation to the reviewers for their helpful comments on this article. This work was supported by Research and Innovation Fund of the First Affiliated Hospital of Harbin Medical University (No. 2017Y013 & 2020YJ01).

Disclosure of conflict of interest

None.

Address correspondence to: Wei Zhang, Department of Respiratory Medicine, The First Affiliated Hospital of Harbin Medical University, No. 23, Youzheng Street, Nangang District, Harbin 150001, Heilongjiang Province, P. R. China. Tel: +86-0451-85556-000; E-mail: zhangweihydyy@163.com

References

[1] Siegel RL, Miller KD and Jemal A. Cancer statistics, 2015. CA Cancer J Clin 2015; 65: 5-29.

[2] Ferlay J, Soerjomataram I, Dikshit R, Eser S, Mathers C, Rebelo M, Parkin DM, Forman D and Bray F. Cancer incidence and mortality worldwide: sources, methods and major patterns in GLOBOCAN 2012. Int J Cancer 2015; 136: E359-386.

[3] Rothschild SI. Advanced and metastatic lung cancer - what is new in the diagnosis and therapy?. Praxis (Bern 1994) 2015; 104: 745-750.

[4] Cline SD and Hanawalt PC. Who's on first in the cellular response to DNA damage? Nat Rev Mol Cell Biol 2003; 4: 361-372.

[5] Li L, Zhu T, Gao YF, Zheng W, Wang CJ, Xiao L, Huang MS, Yin JY, Zhou HH and Liu ZQ. Targeting DNA damage response in the radio (Chemo) therapy of non-small cell lung cancer. Int J Mol Sci 2016; 17: 839.

[6] Collins LG, Haines C, Perkel R and Enck RE. Lung cancer: diagnosis and management. Am Fam Physician 2007; 75: 56-63.

[7] Migheli F and Migliore L. Epigenetics of colorectal cancer. Clin Genet 2012; 81: 312-318.

[8] Davalos V and Esteller M. Disruption of long noncoding RNAs targets cancer hallmark pathways in lung tumorigenesis. Cancer Res 2019; 79: 3028-3030.

[9] Hashemi M, Moazeni-Roodi A, Sarabandi S, Karami S and Ghavami S. Association between

genetic polymorphisms of long noncoding RNA H19 and cancer risk: a meta-analysis. J Genet 2019; 98: article 81.

[10] Xu JL, Hua T, Ding J, Fan Y, Liu ZJ and Lian JW. FOXF2 aggravates the progression of non-small cell lung cancer through targeting lncRNA H19 to downregulate PTEN. Eur Rev Med Pharmacol Sci 2019; 23: 10796-10802.

[11] Cui J, Mo J, Luo M, Yu Q, Zhou S, Li T, Zhang Y and Luo W. c-Myc-activated long non-coding RNA H19 downregulates miR-107 and promotes cell cycle progression of non-small cell lung cancer. Int J Clin Exp Pathol 2015; 8: 12400-12409.

[12] Xu JL, Hua T, Ding J, Fan Y, Liu ZJ and Lian JW. FOXF2 aggravates the progression of non-small cell lung cancer through targeting lncRNA H19 to downregulate PTEN. Eur Rev Med Pharmacol Sci 2019; 23: 10796-10802.

[13] Pan R and Zhou H. Exosomal transfer of lncRNA H19 promotes erlotinib resistance in non-small cell lung cancer via miR-615-3p/ATG7 axis. Cancer Manag Res 2020; 12: 4283-4297.

[14] Zheng ZH, Wu DM, Fan SH, Zhang ZF, Chen GQ and Lu J. Upregulation of miR-675-5p induced by lncRNA H19 was associated with tumor progression and development by targeting tumor suppressor p53 in non-small cell lung cancer. J Cell Biochem 2019; 120: 18724-18735.

[15] Feng Y, Yang C, Hu D, Wang X and Liu X. miR-675 promotes disease progression of non-small cell lung cancer via activating NF-kappaB signaling pathway. Cell Mol Biol (Noisy-le-grand) 2017; 63: 7-10.

[16] Yang L, Li L, Zhou Z, Liu Y, Sun J, Zhang X, Pan H and Liu S. SP1 induced long non-coding RNA LINC00958 overexpression facilitate cell proliferation, migration and invasion in lung adenocarcinoma via mediating miR-625-5p/CPSF7 axis. Cancer Cell Int 2020; 20: 24.

[17] Goyal A, Fiskin E, Gutschner T, Polycarpou-Schwarz M, Gross M, Neugebauer J, Gandhi M, Caudron-Herger M, Benes V and Diederichs S. A cautionary tale of sense-antisense gene pairs: independent regulation despite inverse correlation of expression. Nucleic Acids Res 2017; 45: 12496-12508.

[18] Jin F, Zhu H, Shi F, Kong L and Yu J. A retrospective analysis of safety and efficacy of weekly nab-paclitaxel as second-line chemotherapy in elderly patients with advanced squamous non-small-cell lung carcinoma. Clin Interv Aging 2016; 11: 167-173.

[19] Murphy SK, Huang Z, Wen Y, Spillman MA, Whitaker RS, Simel LR, Nichols TD, Marks JR and Berchuck A. Frequent IGF2/H19 domain epigenetic alterations and elevated IGF2 expression in epithelial ovarian cancer. Mol Cancer Res 2006; 4: 283-292.

[20] Lei Y, Guo W, Chen B, Chen L, Gong J and Li W. Tumorreleased lncRNA H19 promotes gefitinib resistance via packaging into exosomes in nonsmall cell lung cancer. Oncol Rep 2018; 40: 3438-3446.

[21] Huang Z, Lei W, Hu HB, Zhang H and Zhu Y. H19 promotes non-small-cell lung cancer (NSCLC) development through STAT3 signaling via sponging miR-17. J Cell Physiol 2018; 233: 6768-6776.

[22] Forment JV, Blasius M, Guerini I and Jackson SP. Structure-specific DNA endonuclease Mus81/Eme1 generates DNA damage caused by Chk1 inactivation. PLoS One 2011; 6: e23517.

[23] Ohashi S, Kikuchi O, Nakai Y, Ida T, Saito T, Kondo Y, Yamamoto Y, Mitani Y, Nguyen Vu TH, Fukuyama K, Tsukihara H, Suzuki N and Muto M. Synthetic lethality with trifluridine/tipiracil and checkpoint kinase 1 inhibitor for esophageal squamous cell carcinoma. Mol Cancer Ther 2020; 19: 1363-1372.

[24] Bai J, Wang Y, Wang J, Zhai J, He F and Zhu G. Irradiation-induced senescence of bone marrow mesenchymal stem cells aggravates osteogenic differentiation dysfunction via paracrine signaling. Am J Physiol Cell Physiol 2020; 318: C1005-C1017.

[25] Zhang X, Ji S, Cai G, Pan Z, Han R, Yuan Y, Xu S, Yang J, Hu X, Chen M, Wu M, Ma Y, Deng J, Gao X, Guan S, Xu S, Shuai Z, Laslett L and Pan F. H19 increases IL-17A/IL-23 releases via regulating VDR by interacting with miR675-5p/miR22-5p in ankylosing spondylitis. Mol Ther Nucleic Acids 2020; 19: 393-404.

[26] Matouk IJ, Halle D, Gilon M and Hochberg A. The non-coding RNAs of the H19-IGF2 imprinted loci: a focus on biological roles and therapeutic potential in Lung Cancer. J Transl Med 2015; 13: 113.

[27] Wang J, Zhao YC, Lu YD and Ma CP. Integrated bioinformatics analyses identify dysregulated miRNAs in lung cancer. Eur Rev Med Pharmacol Sci 2014; 18: 2270-2274.

[28] Lu Y, Song S, Jiang X, Meng Q, Wang C, Li X, Yang Y, Xin X, Zheng Q, Wang L, Pu H, Gui X, Li T and Lu D. miR675 accelerates malignant transformation of mesenchymal stem cells by blocking DNA mismatch repair. Mol Ther Nucleic Acids 2019; 14: 171-183.

[29] Lucas C, Salesse L, Hoang MHT, Bonnet M, Sauvanet P, Larabi A, Godfraind C, Gagniere J, Pezet D, Rosenstiel P, Barnich N, Bonnet R, Dalmasso G and Nguyen HTT. Autophagy of intestinal epithelial cells inhibits colorectal carcinogenesis induced by colibactin-producing

escherichia coli in Apc(Min/+) Mice. Gastroenterology 2020; 158: 1373-1388.
[30] Dao R, Wudu M, Hui L, Jiang J, Xu Y, Ren H and Qiu X. Knockdown of lncRNA MIR503HG suppresses proliferation and promotes apoptosis of non-small cell lung cancer cells by regulating miR-489-3p and miR-625-5p. Pathol Res Pract 2020; 216: 152823.
[31] Cao L, Cheng H, Jiang Q, Li H and Wu Z. APEX1 is a novel diagnostic and prognostic biomarker for hepatocellular carcinoma. Aging (Albany NY) 2020; 12: 4573-4591.
[32] Wang L, Chen R and Zhang Y. miR-296-3p targets APEX1 to suppress cell migration and invasion of non-small-cell lung cancer. Oncol Lett 2019; 18: 2612-2618.

Supplementary Table 1. Sequences for siRNAs

siRNAs	Sequence
si-H19#1	5'-GCAAGAAGCGGGTCTGTTTCT-3'
si-H19#2	5'-GACAAGCAGGACATGACATGG-3'
si-H19#3	5'-GCACTACCTGACTCAGGAATC-3'
si-NC	5'-TTCTCCGAACGTGTCACGTTT-3'

Note: si/siRNA, short interfering RNA.

Supplementary Table 2. Primer sequences for RT-qPCR

	Forward (5'-3')	Reverse (5'-3')
miR-675	CCCAGGGTCTGGTGCGGAGA	CCCAGGGGCTGAGCGGTGAG
miR-625-5p	GTAGAGGGATGAGGGGGAA	CTCTACAGCTATATTGCCAGCCA
U6	GCTTCGGCAGCACATATACT	GGAACGCTTCACGAATTTGC
H19	ATCGGTGCCTCAGCGTTCGG	CTGTCCTCGCCGTCACACCG
p62	GCAGTATCCCAAGTTCAATT	TGGGAACAGGTGGTGGAGGA
APEX1	TGAAGCCTTTCGCAAGTTCCT	TGAGGTCTCCACACAGCACAA
GAPDH	GCACCGTCAAGGCTGAGAAC	ATGGTGGTGAAGACGCCAGT

Note: RT-qPCR, reverse transcription-quantitative polymerase chain reaction.